Available online at www.sciencedirect.com

SciVerse ScienceDirect

Ceramics International 38 (2012) 3649–3657

CERAMICS INTERNATIONAL

www.elsevier.com/locate/ceramint

Chemical solution deposition of ZnO nanostructure films: Morphology and substrate angle dependency

Farid Jamali-Sheini *

Department of Physics, Ahwaz Branch, Islamic Azad University, Ahwaz, Iran

Received 5 November 2011; received in revised form 17 December 2011; accepted 2 January 2012
Available online 21 January 2012

Abstract

A chemical solution deposition method was used to synthesize ZnO films on zinc foil utilizing an electrolyte of $ZnCl_2 + H_2O_2$ under ambient conditions. The structures, morphologies, and chemical compositions of the films were characterized using X-ray diffractometry (XRD), scanning electron microscopy (SEM), energy-dispersive X-ray spectrometry (EDS), and X-ray photoelectron spectroscopy (XPS) techniques. The XRD patterns showed that the substrate angle had significant influences on the formation of $Zn(OH)_2$ and the transition to ZnO. The SEM observations revealed that the cauliflower-like and rod-like morphologies were altered to one that was disk-like by changing the substrate angle from 90° to 0°. The XPS and EDS results indicated the presence of Cl atoms with a substrate angle of 0°. The XPS data confirmed the chemical purity of the ZnO film on the substrate with 90°. Photoluminescence (PL) studies found different visible emissions originating from different defect mechanisms. The growth mechanism responsible for the variation in the morphology is discussed. The observed results showed that the variation of pH in the vicinity of the surface substrates can be considered as reason for changing of morphology with the variation of angle. This method may have a potential in the fabrication of other metal oxides at low cost for technological applications.

Keywords: Chemical synthesis; Nanostructures; Crystal growth

1. Introduction

The physical and chemical properties of ZnO nanostructures can be altered by changing the morphological and structural parameters such as the shape, size, orientation, and crystallinity of the synthesized materials. Therefore, from the viewpoint of fundamental studies and practical applications, developing a shape-controlled ZnO synthesis method is still a real challenge.

Over the past few years, various kinds of nanostructures have been synthesized using a large number of techniques. Among these, zinc oxide (ZnO) nanostructures have received considerable attention because of their properties, including a wide direct band gap energy (3.37 eV) and large excitation binding energy (60 meV), which suggest numerous possible practical applications. In addition, ZnO seems to have the richest family of nanostructures among all of the materials tested, including particles, rods, tubes, wires, nails, belts, marigolds/multipods, flowers, rings, helixes/springs, etc. [1–8].

Various synthesis methods have been used to fabricate ZnO nanostructures, which can be classified into two categories: vapor-phase [3–8] and solution-phase syntheses [1,2,9–20]. In solution-phase synthesis, a variety of methods such as electrochemical deposition, hydrothermal/solvothermal synthesis, and chemical solution deposition (CSD) have been used to fabricate ZnO nanostructure thin films. Electrochemical deposition requires conductive substrates, while high pressure equipment is needed for hydrothermal/solvothermal method. Among these different methods, CSD, which is also called chemical bath deposition, has been demonstrated to be a simple, inexpensive, and low temperature method for synthesizing ZnO nanostructure films. Many efforts have been made to synthesize ZnO nanoforms by adjusting effective parameters in the CSD method such as the concentration and type of precursor [13–16], additive concentration [17], time and temperature of growth [18,19], substrate [14,16,20], and so on. In addition, this method has been demonstrated to be a facile approach to fabricating large-area ZnO nanostructure films.

* Tel.: +98 611 3348420 24; fax: +98 611 3329200.
E-mail addresses: faridjamali@iauahvaz.ac.ir, faridjamali2003@yahoo.com.

0272-8842/$36.00
doi:10.1016/j.ceramint.2012.01.004

However, the precise control of the ZnO crystal evolution in the CSD process is a formidable task, and the mechanism for the formation of ZnO crystals is hardly understood. Moreover, to the best of our knowledge, there has been no study on the effect of the substrate angle on the growth of ZnO nanostructure films using the CSD method.

Therefore, the aim of this study was to investigate the effects of different substrate angles on the structures, morphologies, and photoluminescence properties of synthesized ZnO nanostructure films.

2. Experimental procedure

2.1. Film preparation

The growth of the ZnO nanostructure films on Zn substrates was performed with a chemical solution deposition technique, using a mixture of $ZnCl_2$ and H_2O_2 (analytical grade), with concentrations of 0.016 M and 0.04 M, respectively. The electrolyte (mixed solution) was stirred for 5 min and placed in a glass beaker with a suitable cap. After one hour, the substrates were placed at the bottom of the beaker and fixed at 0°, 30°, and 90° angles with respect to the solution surface. These samples are called D(0), D(30), and D(90), respectively. A schematic diagram of the experimental setup is shown in Fig. 1. Prior to each experiment, the polycrystalline Zn foil (size: 1 cm × 2 cm and purity: ~99.99%, Alfa Aesar) was ultrasonically cleaned in acetone and methanol (10 min in each solvent). The glass beaker was placed in a dark area at room temperature for 9 days. After the induction period, the specimens were thoroughly washed in a gentle flow of distilled water and dried in air at 50 °C for 5 min. At least three specimens for each angle were synthesized under identical experimental conditions and characterized by analytical techniques to verify the reproducibility and repeatability of the results.

2.2. Characterization

The structures and morphologies of the films were characterized using an X-ray diffractometer (XRD, Model-D8, Advance, Bruker AXS) and scanning electron microscope (SEM, JOEL, JSM-6360A). The elemental composition was obtained using an energy-dispersive X-ray spectrometer (EDS) attached to the SEM. The XRD was used in the 2θ mode, i.e., (20°–80°), with an operating voltage of ~20 kV and Cu Kα (λ: 1.5406 Å) as the radiation source. The SEM images were recorded with an accelerating voltage of ~20 kV and filament current of ~60 μA. The EDS spectra were obtained from at least 4 or 5 different spots (total area ~25 μm^2), with a collection duration of ~80 s for each spot. The EDS spectrometer was calibrated using a standard specimen of gold. The optical properties were investigated using the photoluminescence (PL) spectra recorded at room temperature. The PL was measured with a Perkin Elmer-LS-55 photoluminescence spectrometer, using a Xenon lamp as the source, with an excitation wavelength of ~325 nm. A chemical analysis of the films was performed using X-ray photoelectron spectroscopy (XPS, VG Microtech ESCA 3000). The XPS spectra were recorded at an instrument resolution of ±0.2 eV and a base pressure of 10^{-10} mbar, using Mg Kα radiation (1253.6 eV, line width 0.7 eV) generated at a power of 150 W.

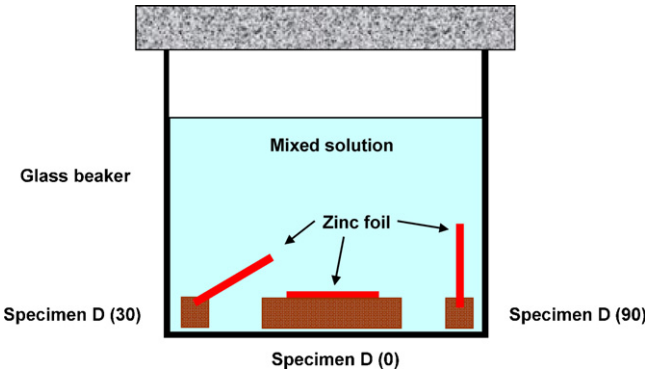

Fig. 1. Schematic diagram of glass beaker, along with different substrate angles for chemical solution deposition of ZnO nanostructure films.

3. Results and discussion

3.1. Structural, morphological, and compositional analyses

The XRD patterns of specimens D(90), D(30), and D(0) are shown in Fig. 2. All of the XRD patterns exhibit a set of well defined diffraction peaks that can be indexed to the wurtzite hexagonal phase of ZnO and $Zn(OH)_2$ by comparing the observed d-values with the standard JCPDS data [21]. Because of the low thermal energy available, the Zn $(OH)_2$ was not completely decomposed to form ZnO. Significant peaks from $Zn_5(OH)_8Cl_2$ were also observed for specimen D(0). The presence of the diffraction peaks corresponding to Zn was a result of using Zn foil as a substrate. It can be seen that the intensity of the ZnO peaks was enhanced with a decrease in the intensity of $Zn(OH)_2$. Accordingly, it is interesting to note that

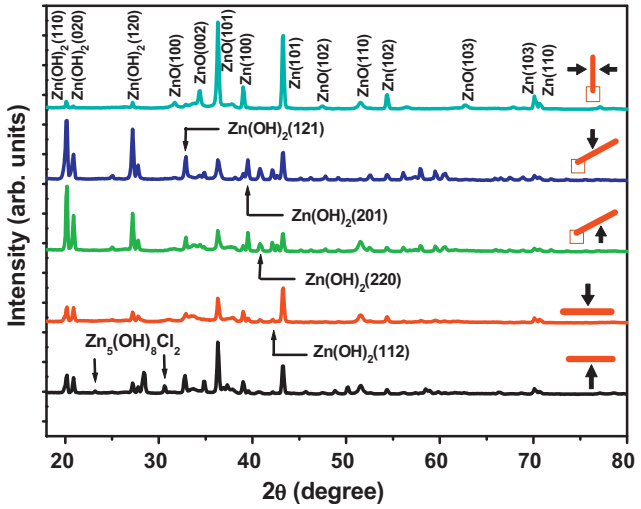

Fig. 2. XRD patterns of ZnO nanostructure films grown with different substrate angles.

the intensity of the diffraction peaks corresponding to the $Zn(OH)_2$ phase is smaller for specimen D(90), suggesting a better formation of ZnO films than in the other specimens.

The SEM images of the synthesized ZnO films with different substrate angles are shown in Fig. 3. It can be seen that the substrate angles effectively influenced the morphologies of the synthesized ZnO films. Several different types of ZnO morphologies are clearly observed in the SEM images. Fig. 3a shows SEM images of specimen D(90). A cauliflower-like morphology was deposited on the zinc substrate. It can be seen that a rod-like morphology, with diameters of about 500 nm–2 μm and a length of several micrometers, formed between the cauliflowers. In the case of specimen D(30), the surface morphologies show the sharp-edge grains (cuboidal particles) on the surface of both sides, as shown in Fig. 3b. Two distinct morphologies are seen on the surface of specimen D(0) (Fig. 3c): a compact and uniform disk-like morphology, with widths of about 5–30 μm and thicknesses of 200–800 nm, on the entire backside of the substrate, and an agglomeration of particles on the entire front side of the substrate. From the XRD and SEM results, one can suggest that when the substrate angle increases from 0° to 90°, the formation/orientation of the obtained structure significantly changes. This effect may be caused by a different formation rate for ZnO nuclei and the aggregation of these nuclei on the zinc substrate.

The chemical purity of the synthesized ZnO films, as well as their stoichiometry, was investigated in an analysis using the EDS attached to the SEM. The average values were determined,

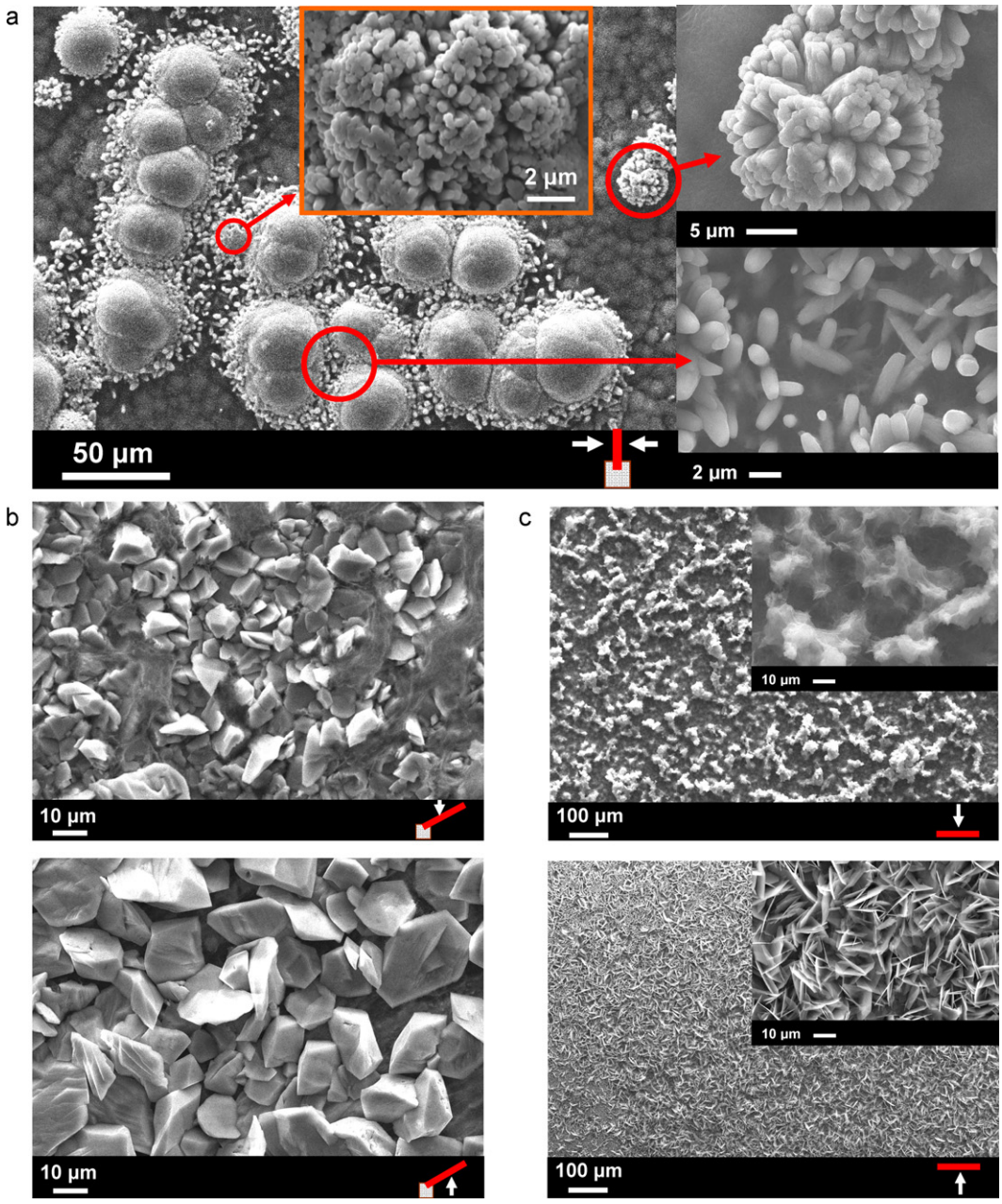

Fig. 3. Low and high magnification SEM images of ZnO nanostructures grown with different substrate angles, (a) 90°, (b) 30°, and (c) 0°, after 9 days deposition.

and a comparison of the data for all of the specimens is presented in Table 1. The results show that specimens D(90) and D(30) are composed only of Zn and O, while Cl is present in specimen D(0), at an atomic percentage of 2–6%.

The chemical composition of each specimen was checked using the XPS technique. This technique can provide a quantitative analysis of the elements within a few nanometers of a film's surface. Fig. 4 shows the XPS spectra for specimen D(90). As can be observed from the survey scan spectrum in Fig. 4a, only the core level photoemission peaks corresponding to zinc, oxygen, and carbon could be seen. Thus, the purity of the specimen was confirmed within the sensitivity range of the technique. The positions for all of the peaks were corrected with respect to those of the C-1s photoemission peak at 285.0 eV as an internal reference, and Au-4f at 84.0 eV as an external reference. Fig. 4b shows a detailed scan of the Zn-2p region. The Zn-$2p_{3/2}$ peak appears at 1021.9 eV and that for Zn-$2p_{1/2}$ appears at 1044.9 eV with a spin orbit splitting of 23.0 eV, confirming that the Zn species is in a completely oxidized state [22]. The peak is symmetric, indicating that no other species such as metallic zinc is present, which would have given a shoulder at ~1021.1 eV [22]. The core level photoemission peak for the O-1s region is given in Fig. 4c. The peak exhibited at 531.5 eV is attributed to the oxidized metal ions in the films, namely O–Zn in the ZnO lattice. Along with zinc and oxygen, some amount of carbon was found in the specimen, which could be the result of specimen handling and some carbon migration from the filaments in the vacuum system. Fig. 5(a–d) shows the detailed XPS scan of the backside of specimen D(0). The survey scan (Fig. 5a) shows the presence of Cl atoms on the surface of this specimen, which are not observed in specimen D(90). The peaks located at 1021.4 eV and 1044.4 eV in Fig. 5b correspond to the Zn-$2p_{3/2}$ and Zn-$2p_{1/2}$ binding energies for ZnO, respectively. The core level photoemission peak for the O-1s region is located at 531.2 eV (Fig. 5c). Deconvoluted

Table 1
EDS results for ZnO nanostructures grown with different substrate angles.

Specimen	Location of analysis	Atomic percentage (at.%) (average)		
		Zn	0	Cl
D(90)	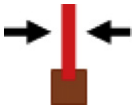	50	50	–
D(30)		63	37	–
	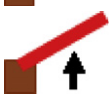	54	46	–
D(0)		54	44	2
		52	42	6

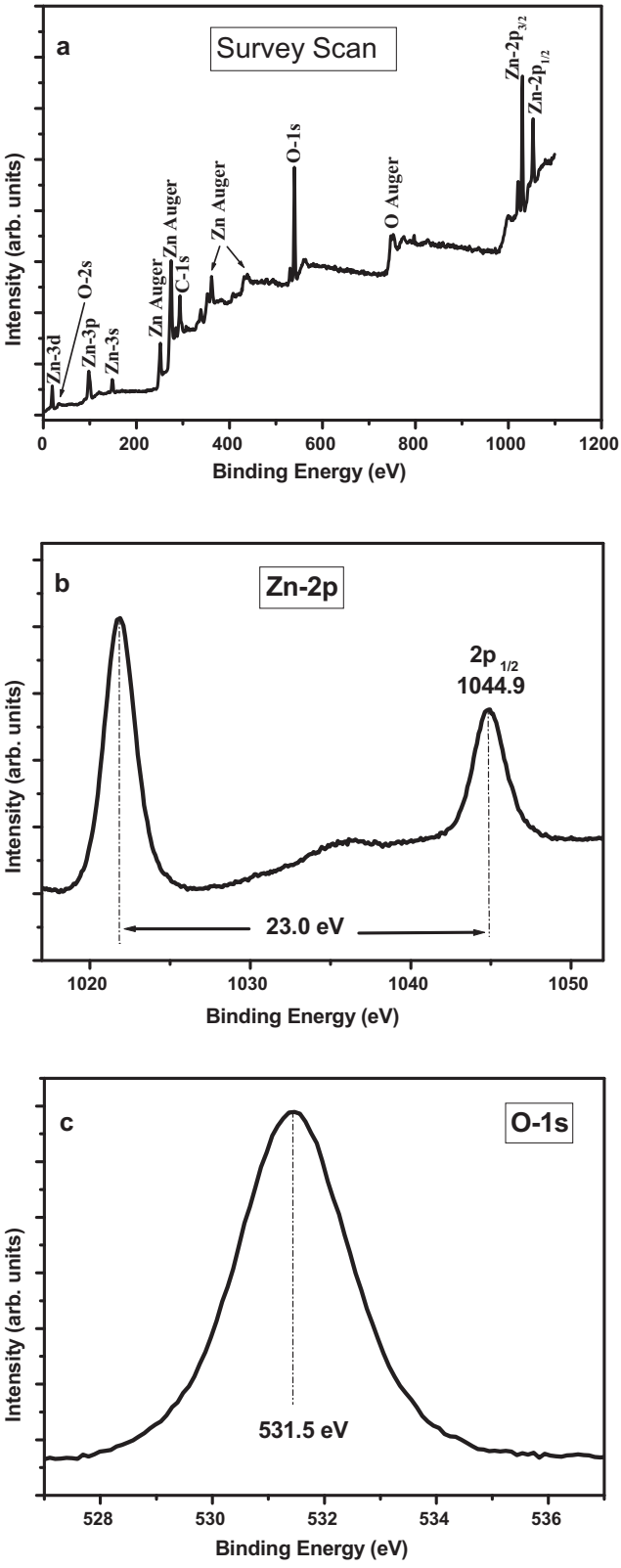

Fig. 4. XPS spectra of specimen D(90): (a) survey scan, (b) Zn-2p region, and (c) O-1s region.

asymmetric peaks for Cl-2p are located at 198.2 eV and 199.8 eV, as shown in Fig. 5d. The lower energy peak is attributed to Cl atoms adsorbed on the surface of the film and the higher peak is believed to be the Cl in the ZnO lattice and

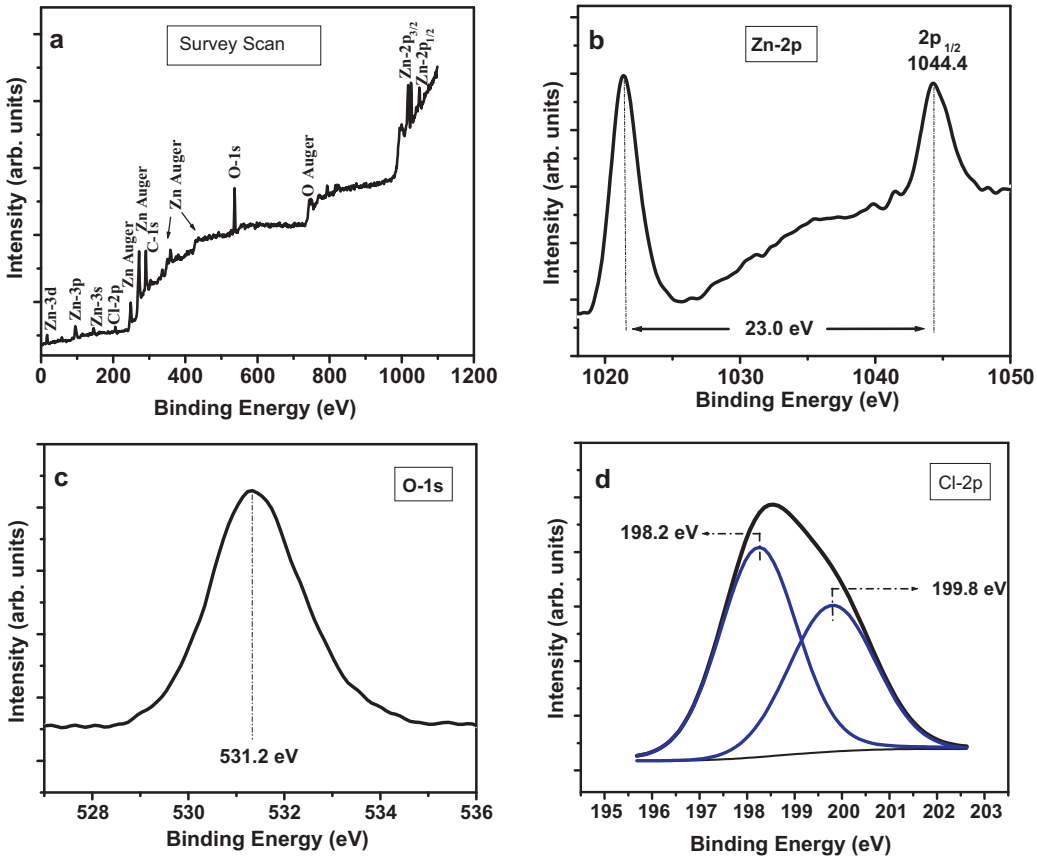

Fig. 5. XPS spectra of specimen D(0): (a) survey scan, (b) Zn-2p region, (c) O-1s region, and (d) Cl-2p region.

unreacted $ZnCl_2$ [22]. This result is in good agreement with the result of the EDS analysis.

3.2. Growth mechanism

The growth of the synthesized ZnO films from an electrolyte (mixed solution) was based on the formation of a solid-phase from the aqueous solution, which includes two steps: (i) nucleation and (ii) growth.

(i) Nucleation

Nucleation can occur by oxidation and reduction of Zn foil and the H_2O_2 on the surface of substrates. It may be suggested that the following reactions are involved in the creation of the primary nucleus.

$$Zn(s) \rightarrow Zn^{2+}(aq) + 2e^- \quad (1)$$

$$H_2O_2 + 2e^- \rightarrow 2OH^-(aq) \quad (2)$$

$$Zn(s) + H_2O_2(aq) \rightarrow Zn^{2+}(aq) + 2OH^-(aq) \rightarrow Zn(OH)_2(s) \quad (3)$$

With an increase in the pH:

$$Zn(OH)_2\,(s) + 2OH^-\,(aq) \rightarrow Zn(OH)_4^{2-} \rightarrow ZnO(s) + 2H_2O \quad (4)$$

During the deposition, the surface of the zinc foil is dissolved by oxidation (reaction (1)), and the H_2O_2 is reduced to OH^- ions (reaction (2)). In this step, $Zn(OH)_2$ (s) is made, which is required for the formation of $Zn(OH)_4^{2-}/Zn(OH)_2/ZnO$ structures as nucleation sites (reactions (3) and (4)). Developing the growth units ($Zn(OH)_4^{2-}$) can act as building blocks incorporated into the crystal lattice. It may be explained that the morphologies of the structures are governed by the nucleation rates for new 2D islands on the surfaces.

(ii) Growth

In the next step, $ZnCl_2$ provides Zn^{2+} ions and creates a $[Zn(H_2O)_xCl_2]$ complex in the electrolyte. This complex can react with the OH^- (aq) that was produced during the nucleation step. When the concentration of the OH^- (aq) and/or the pH is increased, OH^- (aq) ions can replace the H_2O and Cl in the complex. Based on the concentration of OH^- (aq) in the vicinity of the substrate, three different reactions can be considered.

$$[Zn(H_2O)_xCl_2] + (2+x)\,OH^-\,(aq) \rightarrow [Zn(OH)_{(2+x)}]^{(x)-} + x\,H_2O + 2Cl^-\,(aq) \rightarrow ZnO + \ldots\ldots \quad (a)$$

$$[Zn(H_2O)_xCl_2] + (1+x)OH^-(aq) \rightarrow [Zn(OH)_xCl]^{(x-1)-} + xH_2O + Cl^-(aq) \quad (b)$$

$$[Zn(H_2O)_xCl_2] + (x)OH^-(aq) \rightarrow [Zn(OH)_xCl_2]^{(x)-} + xH_2O \quad (c)$$

Therefore, looking at the results for some specimens, one can see that with a lower concentration of OH^-, there is more Cl on the zinc foil surface (reactions (b) and (c), which can be related to the front and backside of D(0), respectively). In contrast, with an increase in the concentration of OH^- and/or pH, the percentage of Cl in the product decreases or cannot be observed (reaction (a) can be attributed to D(30) and D(90)). This explanation was confirmed by pH measurements after 7 days of immersion. The pH was 8.9, 10.1, and 10.3 for D(0), D(90), and D(30), respectively.

With careful observations of the XRD spectra, it can be seen that the intensity of the peaks corresponding to the $Zn(OH)_2$ phases were varied, i.e., with an increase in the intensity of the $Zn(OH)_2$ phases, the intensity of the ZnO phases decreased. This means that the possible decomposition of $Zn(OH)_2$ to ZnO is larger. Yamabi & Imai, and Peterson et al. [23,24] showed that $Zn(OH)_2$ is predominantly formed when the pH is 6–9, while the wurtzite ZnO structure forms at a pH of 9–13. In the present study, although the deposition conditions such as the reactant concentration, growth temperature, and pH of the electrolyte were fixed in the initial stage, the firm conclusion from the XRD results is that the pH level in the vicinity of the substrates can be changed, resulting in the presence of different intensities/formations of $Zn(OH)_2$ and ZnO. Therefore, it is observed that because of different rates of decomposition from $Zn(OH)_2$ to ZnO, different morphologies could be controllably obtained with a change in the substrate angle. Herein, it can be presumed that there are three rates for the decomposition of $Zn(OH)_2$ to ZnO on the substrates, small, moderate, and large for specimens D(90), D(0), and D(30), respectively. Fig. 6 shows a schematic growth diagram.

To understand the growth mechanism, ZnO films were synthesized under the previous conditions, but the substrates were kept in the electrolyte for 3 days. The SEM images of these synthesized ZnO films are shown in Fig. 7. The ZnO films demonstrated the same morphology for each specimen, in contrast to the deposition for 9 days. A careful observation of the micrographs shows that with an increase in the deposition time, the formed ZnO becomes bigger, thicker, rougher, and, hence, exhibits higher density. In addition, in order to study the effect of solution stirring on the morphology the substrates were kept in the electrolyte for 6 days under identical experimental conditions with constant stirring. The SEM results showed large particles on the surface of substrate for each case. The typical SEM image of ZnO film is shown in Fig. 8. Therefore, it is found that the pH played an important role in altering the shape of obtained products.

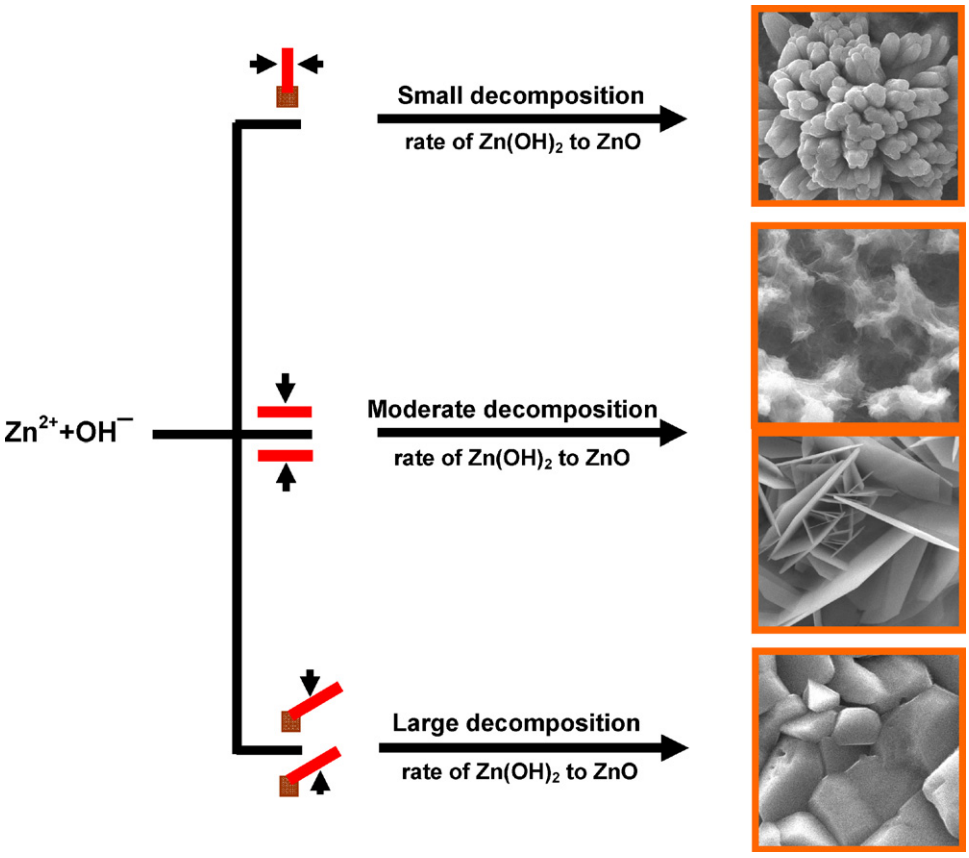

Fig. 6. Schematic growth diagram of ZnO nanostructure films grown with different substrate angles.

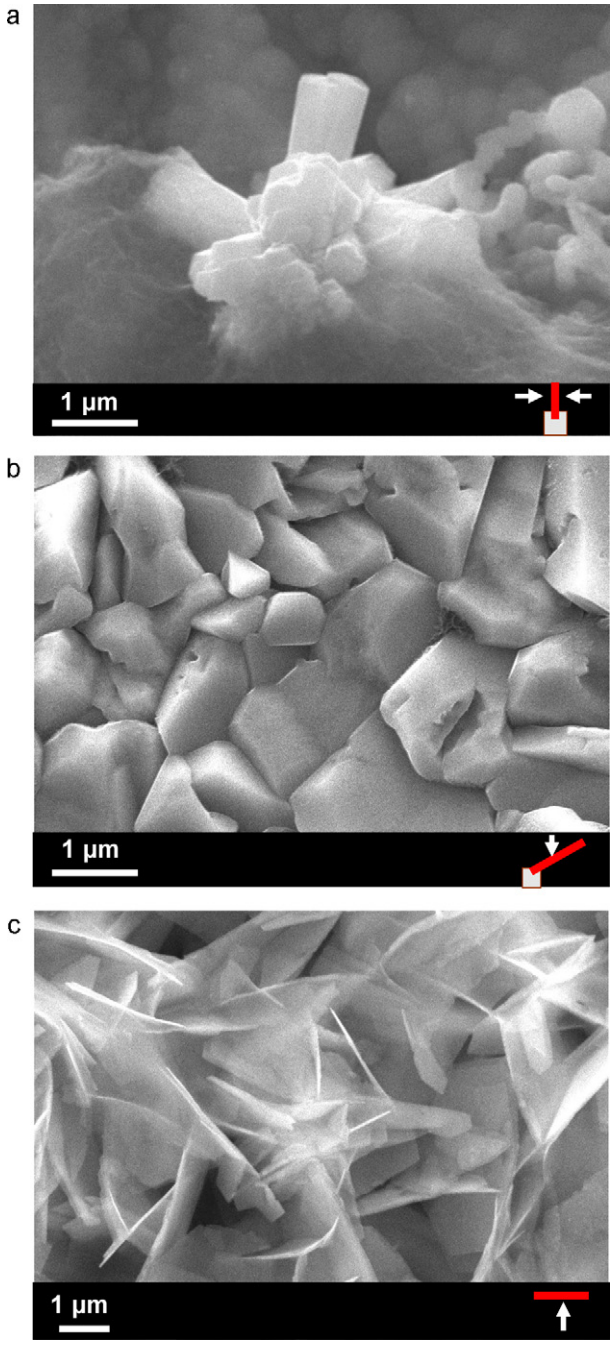

Fig. 7. SEM images of ZnO nanostructures grown with different substrate angles after 3 days deposition.

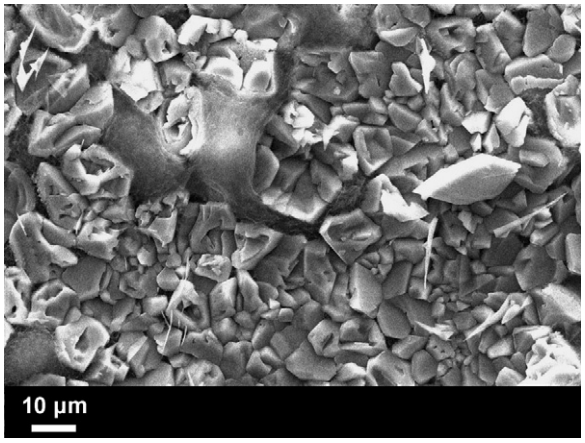

Fig. 8. Typical SEM image of ZnO nanostructures grown after 6 days deposition.

It is well-known that ZnO has a wurtzite structure comprised of a polar crystal with a number of alternating planes composed of tetrahedrally coordinated O^{2-} and Zn^{2+} ions, stacked alternatively along the *c*-axis [25]. The O^{2-} ions are arranged in a hexagonal closed packed (hcp) structure, and each Zn^{2+} is surrounded by four oxygen ions, and vice versa. Thus, ZnO is a polar crystal exhibiting a positively charged plane (0 0 0 1), which is rich in Zn^{2+}, and a negatively charged plane $(0\,0\,0\,\bar{1})$, which is rich in O^{2-}. The anisotropic growth of the ZnO crystal along the [0 0 0 1] direction is caused by the inherent polar properties along the *c*-axis. It has been reported that the most stable crystal of ZnO consists of polar (0 0 0 1), $(0\,0\,0\,\bar{1})$ planes and nonpolar (1 0 0 0) planes [26]. The surface energy of the polar faces is higher than that of the nonpolar faces. Because of the structural anisotropy and surface electronic polarity of ZnO, the surface energies (*E*) of the planes in ZnO crystals are $E(0\,0\,0\,1) > E(1\,0\,\bar{1}\,\bar{1}) > E(1\,0\,\bar{1}\,0) > E(1\,0\,\bar{1}\,1) > E(0\,0\,0\,\bar{1})$ [27]. During the growth process, the surface energy has been ruled out as influencing crystal growth with some preferred planes. In order to reduce the surface energy, the particles are agglomerated to clusters and/or fabricated crystals, with different surface energy. Therefore, the formation of ZnO micro/nano structures may be attributed to the different growth rates of the various crystal planes.

In the case of a cauliflower-like morphology (specimen D(90)), because of the electrostatic force, it can be considered that the negative ions in the electrolyte ($Zn(OH)_4^{2-}$) could be adsorbed on the positive polar plane of (0 0 0 1), resulting in the growth behaviors of the ZnO crystal in the [0 0 0 1] direction, as compared to other growth planes.

In the case of the disk-like morphology (backside of specimen D(0)), the growth rate of the ZnO crystal along the [0 0 0 1] direction decreased, which may have been caused by the adsorption of Cl^- ions from the electrolyte on the $\pm(0\,0\,0\,1)$ planes, resulting in the stabilization of the (0 0 0 1) plane and redirecting the growth on the nonpolar planes in the form of hexagonal disks. Xu et al. and Pradhan & Leung [28,29] suggested that the adsorption of Cl^- on the (0 0 0 1) planes may play an important role in the formation of disks. The presence of Cl was proved by the EDS results, in which the average atomic percentage of Cl was estimated to be 6%. For the front side of specimen D(0), it can be seen that agglomerated particle/cluster structures are fabricated. This specimen shows the presence of Cl with an average atomic percentage of 2%. One could therefore speculate that during the deposition growth, the adsorption of Cl^- on the initial ZnO crystal (nuclei sites of the initial growth stage), prevented further crystallization and the formation of crystalline particles. Here, it may be concluded that, in the electrolyte, there were various amounts of ions with different charges, and that these

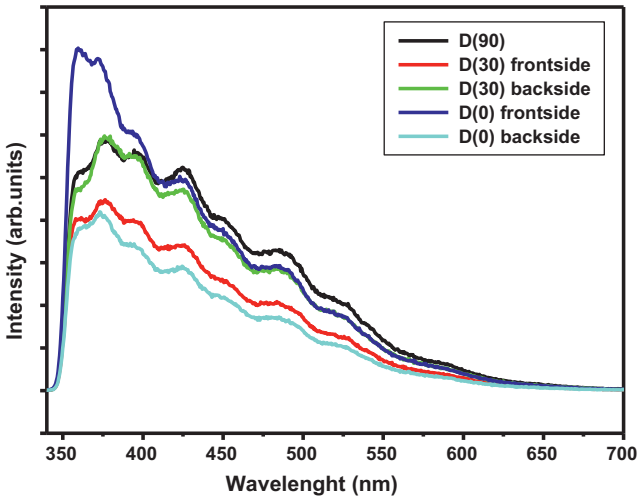

Fig. 9. PL spectra of ZnO nanostructures grown with different substrate angles after 9 days deposition.

charges adsorbed on the surface of each initial ZnO crystal and played an important role in the growth mechanism.

As shown in Fig. 3 for specimen D(30), isolated ZnO particles/grains with well-developed geometrical shapes and sharp edges were present. For the moderate decomposition of $Zn(OH)_2$ to ZnO, the growth rate of the crystal planes may be changed by the addition of adsorbing on the (0 0 0 1) planes.

3.3. Optical properties

In order to investigate the optical properties of the ZnO films, PL measurements were performed at room temperature (Fig. 9). It is clear that all of the specimens showed a similar PL feature with different intensities. Interestingly, the spectra exhibited a broad emission of ~377 nm in the ultraviolet (UV) region and several peaks at ~395, 425, 485, 522, and 590 nm in the near-ultraviolet (NV) and visible regions. The UV peak could be generally attributed to the near-band-edge emission of the ZnO, which originated from the radiative recombination of free excitons between the conduction band and valence band [30]. In addition, it is commonly accepted that the visible emission in ZnO originates from a different deep-level emission located in the band gap such as oxygen vacancies and/or zinc interstitials [31,32]. On the other hand, it is plausible to consider that the broad visible peak is composed of three narrower peaks in the green, yellow, and red emission regions, which originated from different defect mechanisms. Different visible emissions related to the presence of defects appear in the specimens, which could be the result of the low temperature synthesis process. Furthermore, it is well known that the surface state is restricted on the surface of a structure. Thus, the synthesized ZnO films had different morphologies because the surface-to-volume ratio had different values, which in turn affected the PL results. In the present work, the EDS results showed that the atomic percentage of zinc was more than that of oxygen in specimens D(30) and D(0), which indicated that these specimens were Zn-rich. Therefore, the oxygen vacancies would be the main defects in these films.

4. Conclusions

In summary, ZnO with different morphologies such as cauliflower-like, rod-like, disk-like, and sharp-edge grains were successfully fabricated using chemical solution deposition under ambient conditions without using any surfactant, template, or structure-directing solvent. The substrate angle played crucial roles in the $Zn(OH)_2$ to ZnO decomposition rate and the presence of Cl^- ions, resulting in the growth of different morphologies. With a longer growth period without a change in the conditions, the formed ZnO became bigger, thicker, rougher, and exhibited higher density. The results showed that the variation of pH was the main reason for changing the morphology. However, the stirring of electrolyte during reaction time showed the same morphology for each case. Optical studies revealed that different visible emissions originated from different defect mechanisms. This method could be employed to synthesis nano/micro structures in some other metal oxides.

Acknowledgments

This work was financially supported by the Ahwaz Branch of the Islamic Azad University, Ahwaz, Iran. The author is grateful to Prof. P.B. Vidyasagar (Head of Department), Prof. D.S. Joag, and Dr. M.A. More from the Department of Physics, University of Pune, India, and to Dr. K.R. Patil from the National Chemical Laboratory, Pune, India, for their instrumentation support. Thanks also go to Dr. M.R. Mahmodian from the University of Malaya, Malaysia, for the helpful discussion and technical advice for this work.

References

[1] Z. Hu, D.J. Escamilla Ramírez, B.E. Heredia Cervera, G. Skam, P.C. Searson, Synthesis of ZnO nanoparticles in 2-propanol by reaction with water, J. Phys. Chem. B 109 (2005) 11209–11214.
[2] H. Yu, Z. Zhang, M. Han, X. Hao, F. Zhu, A general low-temperature route for large-scale fabrication of highly oriented ZnO nanorod/nanotube arrays, J. Am. Chem. Soc. 127 (2005) 2378–2379.
[3] M.H. Huang, Y. Wu, H. Feick, N. Tran, E. Weber, P. Yang, Catalytic growth of zinc oxide nanowires by vapor transport, Adv. Mater. 13 (2001) 113–116.
[4] F. Jamali Sheini, S.D. Joag, M.A. More, J. Singh, O.N. Srivasatva, Low temperature growth of aligned ZnO nanowires and their application as field emission cathodes, Mater. Chem. Phys. 120 (2010) 691–696.
[5] A. Umar, M.M. Rahman, S.H. Kim, Y.B. Hahn, Zinc oxide nanonail based chemical sensor for hydrazine detection, Chem. Commun. 2 (2008) 166–168.
[6] N.S. Ramgir, D.J. Late, A.B. Bhise, I.S. Mulla, M.A. More, D.S. Joag, V.K. Pillai, Field emission studies of novel ZnO nanostructures in high and low field regions, Nanotechnology 17 (2006) 2730–2735.
[7] X.Y. Kong, Y. Ding, R.S. Yang, Z.L. Wang, Single-crystal nanorings formed by epitaxial self-coiling of polar nanobelts, Science 303 (2004) 1348–1351.
[8] X.Y. Kong, Z.L. Wang, Spontaneous polarization-induced nanohelixes, nanosprings, and nanorings of piezoelectric nanobelts, Nano Lett. 3 (2003) 1625–1631.

[9] S. Peulon, Lincot, Cathodic electrodeposition from aqueous solution of dense or open-structured zinc oxide films, Adv. Mater. 8 (1996) 166–170.
[10] F. Jamali Sheini, I.S. Mulla, D.S. Joag, M.A. More, Influence of process variables on growth of ZnO nanowires by cathodic electrodeposition on zinc substrate, Thin Solid Films 517 (2009) 6605–6611.
[11] Y. Zeng, T. Zhang, W. Fu, Q. Yu, G. Wang, Y. Zhang, Y. Sui, L. Wang, C. Shao, Y. Liu, H. Yang, G. Zou, Fabrication and optical properties of large-scale nutlike ZnO Microcrystals via a low-temperature hydrothermal route, J. Phys. Chem. C 113 (2009) 8016–8022.
[12] B. Wen, Y. Huang, J.J. Boland, Controllable growth of ZnO nanostructures by a simple solvothermal process, J. Phys. Chem. C 112 (2008) 106–111.
[13] L. Vayssieres, Growth of arrayed nanorods and nanowires of ZnO from aqueous solution, Adv. Mater. 15 (2003) 464–466.
[14] K. Govender, D.S. Boyle, P.B. Kenway, P. O'Brien, Understanding the factors that govern the deposition and morphology of thin films of ZnO from aqueous solution, J. Mater. Chem. 14 (2004) 2575–2591.
[15] B. Cao, W. Cai, From ZnO nanorods to nanoplates: chemical bath deposition growth and surface-related emissions, J. Phys. Chem. C 112 (2008) 680–685.
[16] Z. Wang, X.-f. Qian, J. Yin, Z.-k. Zhu, Large-scale fabrication of tower-like, flower-like, and tube-like ZnO arrays by a simple chemical solution route, Langmuir 20 (2004) 3441–3448.
[17] R. Zhang, L.L. Kerr, A simple method for systematically controlling ZnO crystal size and growth orientation, J. Solid State Chem. 180 (2007) 988–994.
[18] Y.-F. Cao, H.-Y. Miao, H.-J. Luo, M. Nagai, J.J. Shyue, Morphological, Crystallographic transformation of ZnO in solution, J. Phys. Chem. C 112 (2008) 1498–1506.
[19] S. Hirano, K. Masuya, M. Kuwabara, Multi-nucleation-based formation of oriented zinc oxide microcrystals and films in aqueous solutions, J. Phys. Chem. B 108 (2004) 4576–4578.
[20] J.-Y. Lee, D. Yin, S. Horiuchi, Site and morphology controlled ZnO deposition on Pd catalyst prepared from Pd/PMMA thin film using UV lithography, Chem. Mater. 17 (2005) 5498–5503.
[21] Powder Diffraction File, International Centre for Diffraction Data, Swarthmore, PA, JCPDS File No. ZnO: 80-0075, $Zn(OH)_2$: 76-1778 and Zn: 01-1244, 1999.
[22] G.E. Muilenbenger (Ed.), Handbook of X-Ray Photoelectron Spectroscopy, Perkin-Elmer Corporation, Minnesota, 1979.
[23] S. Yamabi, H. Imai, Growth conditions for wurtzite zinc oxide films in aqueous solutions, J. Mater. Chem. 12 (2002) 3773–3778.
[24] R.B. Peterson, C.L. Fields, B.A. Gregg, Epitaxial chemical deposition of ZnO nanocolumns from NaOH solutions, Langmuir 20 (2004) 5114–5118.
[25] Z.L. Wang, Zinc oxide nanostructures: growth, properties and applications, J. Phys.: Condens. Matter 16 (2004) R829–R858.
[26] J.Q. Hu, Q. Li, N.B. Wang, C.S. Lee, S.T. Lee, Synthesis of uniform hexagonal prismatic ZnO whiskers, Chem. Mater. 14 (2002) 1216–1219.
[27] L. Xu, Y.-L. Hu, C. Pelligra, C.-H. Chen, L. Jin, H. Huang, S. Sithambaram, M. Aindow, R. Joesten, S.L. Suib, ZnO with different morphologies synthesized by solvothermal methods for enhanced photocatalytic activity, Chem. Mater. 21 (2009) 2875–2885.
[28] L. Xu, Y. Guo, Q. Liao, J. Zhang, D. Xu, Morphological control of ZnO nanostructures by electrodeposition, J. Phys. Chem. B 109 (2005) 13519–13522.
[29] D. Pradhan, K.T. Leung, Controlled growth of two-dimensional and one-dimensional ZnO nanostructures on indium tin oxide coated glass by direct electrodeposition, Langmuir 24 (2008) 9707–9716.
[30] Y.C. Kong, D.P. Yu, B. Zhang, W. Fang, S.Q. Feng, Ultraviolet-emitting ZnO nanowires synthesized by a physical vapor deposition approach, Appl. Phys. Lett. 78 (2001) 407–409.
[31] Y. Kim, R. Seshadri, Optical properties of cation-substituted zinc oxide, Inorg. Chem. 47 (2008) 8437–8443.
[32] V.A.L. Roy, A.B. Djurisic, W.K. Chan, J. Gao, H.F. Lui, C. Surya, Luminescent and structural properties of ZnO nanorods prepared under different conditions, Appl. Phys. Lett. 83 (2003) 141–143.